Research Article

Muhammad Shoaib Bhutta, Yuanhua Chen*, Muneeb Ahmed, Atif Mahmood, Munirah D. Albaqami, Saikh Mohammad, Jee-Hyun Kang, Wail Al Zoubi*, and Dongwhi Choi*

Incorporating GO in PI matrix to advance nanocomposite coating: An enhancing strategy to prevent corrosion

https://doi.org/10.1515/ntrev-2023-0224
received December 26, 2023; accepted February 23, 2024

Abstract: This research endeavors to advance the anti-corrosive characteristics, mainly the physico-mechanical properties, by incorporating graphene oxide (GO) into a polyimide (PI) matrix. So, a nanocomposite coating is fabricated for an aluminum alloy substrate. Results reveal that the coating was uniformly dispersed across the surface signifying that the inclusion of GO increased the PI dispersion. The π–π stacking interactions between the aromatic rings of PI and GO contribute to their stability and improved anticorrosive properties. The incorporation of GO to PI films significantly enhances hydrophobicity, as evidenced by the increased contact angles. Assessing the corrosion resistance of the coating in a 3.5 wt% NaCl solution through electrochemical impedance spectroscopy and potentio-dynamic polarization establishes a prominent correlation between the percentage of GO and the anticorrosion efficiency of the composite coating. Precisely, the nanocomposite coating containing 5 wt% GO exhibits an impressive impedance modulus value of 10^7, and the corrosion current density (I_{cor}) is drastically reduced by over three orders of magnitude, reaching 4.8×10^{-9} A cm^{-2}, as indicated by the polarization curve. Also, prolonged immersion tests confirm the exceptional protective ability of the S_5 coating (5 wt% GO), effectively shielding the metal for up to 100 h. After conducting diagnostic measurements, the hybrid nanocomposites of GO/PI examined in this study showcased their effectiveness as inhibitors in anticorrosive coatings. These composites played a vital role to hinder the oxidation of underlying aluminum alloy when exposed to oxidizing chemicals, water, or air, thereby extending the protective duration.

Keywords: graphene oxide, corrosion resistance, composite coating, active corrosion inhibition

*** Corresponding author: Yuanhua Chen,** School of Automobile Engineering, Guilin University of Aerospace Technology, Guilin, 541004, China; College of Mechanical and Vehicle Engineering, Hunan University, Hunan, 410082, China, e-mail: cyh@guat.edu.cn
*** Corresponding author: Wail Al Zoubi,** Materials Electrochemistry Laboratory, School of Materials Science and Engineering, Yeungnam University, Gyeongsan, 38541, Republic of Korea, e-mail: wailalzoubi@ynu.ac.kr
*** Corresponding author: Dongwhi Choi,** Department of Mechanical Engineering (Integrated Engineering Program), Kyung Hee University, 1732 Deogyeong-daero, Yongin, Gyeonggi, 17104, Republic of Korea, e-mail: dongwhi.choi@khu.ac.kr
Muhammad Shoaib Bhutta: School of Automobile Engineering, Guilin University of Aerospace Technology, Guilin, 541004, China
Muneeb Ahmed: State Key Laboratory of Electrical Insulation and Power Equipment, Xi'an Jiaotong University, Xi'an 710049, China
Atif Mahmood: Faculty of Electrical Engineering, Ghulam Ishaq Khan Institute of Engineering Sciences and Technology, 23460, Topi Swabi, Pakistan
Munirah D. Albaqami, Saikh Mohammad: Department of Chemistry, College of Science, King Saud University, Riyadh, 11451, Saudi Arabia
Jee-Hyun Kang: Materials Electrochemistry Laboratory, School of Materials Science and Engineering, Yeungnam University, Gyeongsan, 38541, Republic of Korea

1 Introduction

Metal corrosion is a key economic and industrial issue, causing deterioration through chemical or electrochemical reactions. Mild steel is favorable across industries due to its remarkable mechanical ability and affordability. The exposure of mild steel to environmental elements can undermine its integrity, prompting the need for corrosion protection. Unfortunately, achieving absolute corrosion prevention is impossible. However, the pragmatic approaches involve controlling corrosion by either slowing down its progression or altering its mechanism [1–3]. Several techniques have been established to protect against corrosion, including cathodic protection, protective coating applications, and the usage of corrosion inhibitors [4–6]. Among them, polymeric protective coatings are highly appreciated for their effectiveness in mitigating the impact of corrosion on metals [7–9].

Polymeric protective coatings are extensively utilized due to their exceptional processability, chemical

resistance, and strong adhesion to metallic surfaces. The involvement of nanoparticles in polymers presents a promising solution by developing corrosion-resistant nanocomposites to overcome these issues [10–12]. The homogenous dispersion of nanoparticles within the polymer matrix establishes strong interactions among the matrix and fillers contributing to enhanced electronic conductivity and corrosion resistance [13,14]. The nanoparticles in anticorrosion coatings develop intricate barriers, thus slowing down corrosive substance diffusion and delaying metallic corrosion [15–17]. Several simple techniques, such as solution methods, spin coating, spray coating, and others, have been employed to fabricate anticorrosion polymer/nanocomposite coatings on metal surfaces [18–20]. The anticorrosion and barrier properties of these coatings depend on achieving a uniform dispersion of nanofillers and establishing favorable interfaces within the nanocomposites. To further improve barrier properties, nanoparticle integration has emerged as a promising route, enhancing anodic/cathodic protection and adhesion [21–23].

Recently, graphene (G) and graphene oxide (GO) have gained researchers' interest due to their impressive attributes – high thermal, electronic, and mechanical properties – making them perfect for various applications. GO, particularly, establishes substantial potential across fields like supercapacitors, electronics, batteries, fuel cells, solar cells, bioscience, biotechnology, and nanosensors [24–27]. Its excellent barrier properties, rooted in high surface area and impermeability, are perfect for thin layers [28–30]. Also, GO serves as a lubricant, minimizing friction and reinforcing wear resistance to mitigate mechanical failure. The GO contains functional groups such as hydroxyl, carbonyl, carboxyl, and epoxide, which offer suitable reaction sites for covalent bonding. Also, GO contains the tendency to interact with water molecules, effectively trapping them and limiting their access to the metal surface [31–33]. Moreover, because of the functional groups presented in GO, it facilitates the covalent or non-covalent bonding which further enhances its compatibility with solvents/polymers [34]. As a result, GO is widely recognized as an excellent nanofiller for preparing composites, particularly in the realm of anticorrosion applications [35–37].

In this study, aromatic polyimide (PI) is used, which has exceptional thermal and mechanical capabilities, strong chemical stability, and distinctive optical features [38,39]. Owing to these remarkable qualities, PI films offer a great deal of potential for cutting-edge uses in the electronics sector [40], including as gas separation membranes [41] and anticorrosion materials [42]. Dorigatoa *et al.* [43] and Gul *et al.* [44] have also proposed the incorporation of PI and nanofillers into epoxy coatings to enhance coating toughness, tensile strength, and flexural modulus and improve the dispersion of nanofillers within the organic coating. Research now focuses on two key areas: first, it aims to further enhance the barrier performance and protective impact of organic composite coatings by improving the dispersion and compatibility of GO in polymer matrix [45]. According to the literature, incorporation of PI films into GO is suggested for the preparation of coatings having improved anticorrosive properties. This work is an attempt to explore the enhancement in physiochemical properties of PI films when bonded with different concentrations of GO nanoparticles.

Due to the anti-corrosion performance of GO nanoparticles and PI films, we prepared composites with different PI/GO wt%. The corrosion resistance of developed coatings is investigated using different diagnostic techniques. To enhance the interaction between PI and GO, a coupling agent called "molecular bridge" is utilized. Surface modification of pyromellitic dianhydride (PMDA) was applied on the PI/GO anti-corrosive composite coating of an aluminum alloy matrix to improve the extent of crosslinking and the functionality of the outer layer of the coating. Fourier transform infrared (FTIR) spectrum is used to inspect the chemical composition of the coatings, while an scanning electron microscope (SEM) is used to investigate the morphology of PI/GO. The anti-corrosion mechanism of pristine PI and PI/GO composites is examined by the electrochemical impedance spectroscopy (EIS) and Tafel polarization techniques.

2 Experimental

2.1 Materials synthesis

The objective of this research study is to fabricate samples of GO and PI nanosheets. For that purpose, we sourced GO nanosheet, 10–50 nm in diameter and one- to two-layer thick (0.334–0.668 nm), from China's Sixth Element Materials Technology Co., Ltd. The necessary materials, including 4,4′-diamino diphenyl ether (ODA), PMDA, and *N*,*N*-dimethylacetamide (DMAc), having 99.8% purity and water content of 30 ppm, were acquired from Alfa Aesar and Thermo Fisher Scientific Co., Ltd., China. Especially, the PMDA underwent vacuum drying for 2 h at 100°C before the reaction.

2.2 Fabrication procedure for PI/GO-based coatings

First, GO was mixed with 100% ethyl alcohol. To create PI films, PMDA and DMAc were gradually added at a

temperature of 25°C with a ratio of 1.02/1 (mol/mol), respectively. The fabrication procedure for PI/GO composite coatings is illustrated in Figure 1. Following the volatilization of the DMAc solvent, imidization was carried out for 30 min at 150, 200, 250, and 300°C. After that, ODA was added to the solution for creating pure PI films. The mixture was then agitated for 2 h while being surrounded by nitrogen to create the PI solution. The produced PI solution was then added, and various amounts of GO suspension (0.1, 0.5, 1, 5, and 10 wt%) were mixed for 1 h at room temperature on the magnetic stirrer. To obtain the protective layer of the coating, the chemical solution was then applied to the metallic surface of the aluminum alloy using the spin coating process and allowed to dry for 6 h at 100°C in a vacuum drying oven (DZF-6020). The list of prepared coatings is represented in Table 1.

Table 1: Symbols and weight percentage of prepared coatings

Sr. #	Coating symbol	Coating composition
1	S_0	100% GO
2	S_1	100% PI film
3	S_2	99.9% PI + 0.1% GO
4	S_3	99.5% PI + 0.5% GO
5	S_4	99% PI + 1% GO
6	S_5	95% PI + 5% GO
7	S_6	90% PI + 10% GO

2.3 Characterization

2.3.1 Morphological observations

The morphological variations in the PI/GO composites with varying concentrations of GO are analyzed using the National Optical Advanced Trinocular LED Microscope and scanning electron microscopy obtained from Thermo Fisher Scientific, Waltham, MA, USA. Prior to the measurements, gold sputtering was applied to the samples. Images with different magnifications have been captured to observe the morphological differences among the composite coatings.

2.3.2 FTIR spectroscopy

The Nicolet FTIR spectroscope (Thermo-fisher Scientific, Waltham, MA, USA) in transmission mode is used to examine the microscopic presence of the function group of PI/GO composites. The

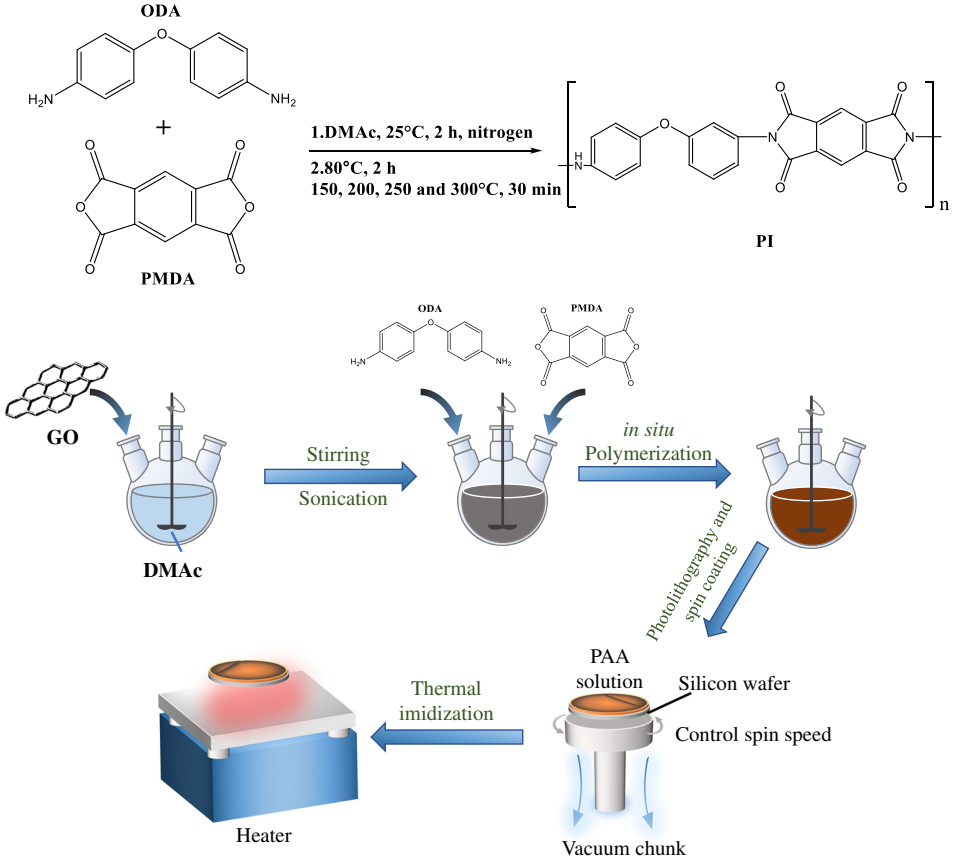

Figure 1: Fabrication procedure for PI/GO composite coatings.

spectral range of 500–4,000 cm^{-1} is considered. For accuracy, the measurement of three samples was considered. The resolution for spectroscopy was better than 0.4 cm^{-1} [46].

2.3.3 X-ray diffraction (XRD)

The crystal structure of composite coatings is examined using the XRD method. The XRD instrument utilized is the D8 ADVANCE-Bruker. The measurements were taken at 80° with an angle rate of 1°/min.

2.3.4 EIS analysis

EIS (three-electrode system) and polarization curve in 3.5 wt% NaCl solution were used to characterize the corrosion properties of the samples. Electrochemical testing was conducted using CHI606 having a three-electrode setup consisting of a platinum counter electrode, a silver/silver chloride reference electrode, and an aluminum plate electrode coated with various coatings as the working electrode. The sample had a surface area of 1 cm^2, and room temperature was used for the test procedure. The EIS test had a frequency range of 10^5–10^{-2} Hz and an amplitude of 10 mV. The polarization curve's voltage range was −1.4 to 0 V, and its scanning rate was 10 mV/s. The samples were all submerged for 30 min prior to the test in a 3.5% NaCl solution.

2.3.5 Tafel polarization analysis

In assessing anticorrosive properties, Tafel polarization was employed. It involves an electrochemical cell with a metal substrate and a counter electrode in a controlled electrolyte environment. By applying different potentials to the metal substrate and measuring resulting current densities, the effectiveness of corrosion inhibitors or coatings can be determined. The Tafel plot derived from this data reveals corrosion kinetics, offering insights into protective mechanisms and material durability.

3 Results and discussion

3.1 Infrared spectrum analysis of PI/GO composite coatings

In Figure 2, the infrared spectrum of S_0, S_1, S_4, and S_6 composites are illustrated. Investigating the distinct infrared spectra

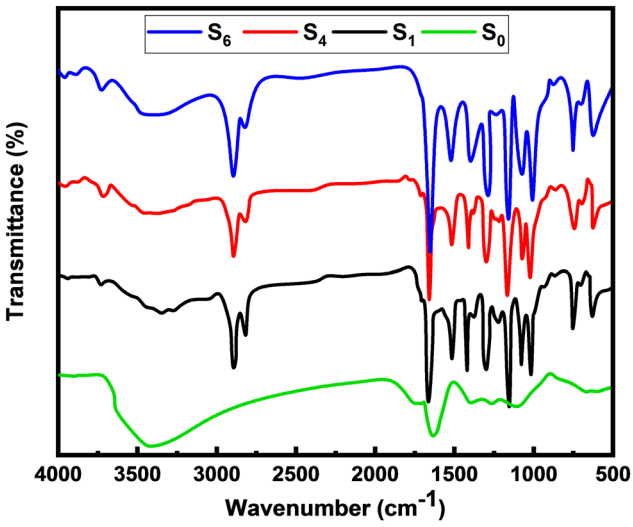

Figure 2: Infrared spectrum of S_0, S_1, S_4, and S_6.

of GO and PI is essential for comprehending the chemical change mechanism within PI/GO composites. In Figure 2, S_0 exhibits a peak for absorption that is both wide and strong at a wavelength of 3,460 cm^{-1}. This peak is connected with the vibration caused by the stretching of the hydroxyl group (OH). Moreover, the vibrations of stretching of C–O and the deformity vibrations of OH in the carboxyl groups are correlated with the peaks of absorptions at 1,740 and 1,400 cm^{-1}, respectively. Asymmetric C–C double bonds, ether bonds, and epoxy groups are confirmed by absorption peaks at 1,260, 1,100, and 1,630 cm^{-1}, respectively [27,33]. Oxidation of GO resulted in a significant increase in functional groups that include oxygen, such as ether bonds, carboxyl, hydroxyl, and epoxy groups. This expansion in function groups created enhanced prospects for subsequent chemical reactions [41].

Figure 2 also reveals the infrared absorption peaks of PI and PI/GO composites. PI (S_1) exhibits hydrophobic features due to its strong bounded molecular structure and high cross-linking among DMAc and ODA. PI contains benzene rings, carboxylic anhydride groups, amino acids, and ethers that allow conducting a wide range of chemical reactions. The blending of PI with GO generates chemical reactions depending on the specific conditions and functional groups. The amino groups ($–NH_2$) present in PI react with the carboxyl groups (–COOH) present in GO, forming amide bonds (–CONH–) and resulting in the attachment of PI chains onto the GO surface. For PI/GO composites, the amino ($–NH_2$) groups typically exhibit characteristic peaks near 3,370 cm^{-1}. This region is known as the "Amide A" or "N-H stretching" region and illustrates strong covalent bonding among PI and GO.

The aromatic rings present in both PI and GO engage in π–π stacking interactions. This non-covalent interaction allows for strong intermolecular bonding between the PI

and GO sheets, leading to improved dispersion and compatibility of PI within the PI matrix. Both PI and GO contain functional groups that can participate in hydrogen bonding. Hydrogen bonds can form between hydroxyl groups (–OH) in GO and amide groups (–CONH–) in PI, enhancing the interfacial interactions between the two materials. Aromatic C–H stretching vibrations typically occur in the range of 2,966 cm^{-1}, while aromatic C═C stretching vibrations typically appear around 1,630 cm^{-1} which can also be seen in FTIR spectrograms.

3.2 Hydrophobicity of PI/GO composite coatings

The contact angles for coatings of PI and PI/GO composites are shown in Figure 3. As seen in Figure 3, the highest contact angle of 121° was recorded for S_5 (5% nano-GO) and the lowest contact angle of 92° was for pristine PI, i.e., S_1. It is found that the coated surface's contact angle without a coupling agent was 92°, indicating the hydrophobic characteristics of PI films. The alloying of GO nanoparticles in the PI matrix can further enhance the contact angle specifying better hydrophobicity of PI/GO composites. In other words, upon incorporating GO concentrations into the PI matrix, the nanofillers dispersed uniformly, revealing no visible agglomeration. The introduction of GO resulted in a rough surface for PI/GO composites, contributing to improved hydrophobicity which is also reported in ref. [47]. If the contact angle of coating is below 90°, then it will be hydrophilic, permitting water molecules to accumulate on the surface and infiltrate the metal through diffusion channels, thereby accelerating metal corrosion. The anti-corrosive nature of the coating is significantly influenced by PI's low surface energy and its rough surface structure. The hydrophobic surface, which prevents the adsorption of water molecules and corrosive ions, helps minimize the infiltration of ions into metal substrates through the coating [48]. The anti-corrosion components and hydrophobic surface structure give a dual protection mechanism for aluminum. The increase in contact angle to 121° for sample S_5 is much higher than the contact angle of 102° in a recently reported study employing 5% GO into epoxy resins [49].

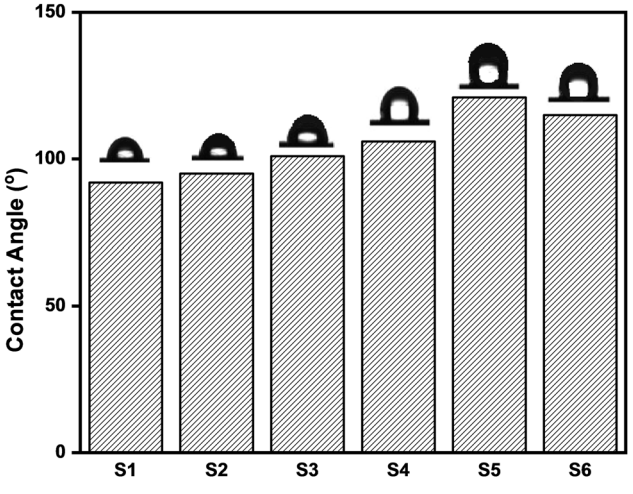

Figure 3: Contact angle of prepared composites showing the increased hydrophobicity with the addition of GO nanoparticles.

3.3 Morphological analysis of PI/GO composites

The dispersion of PI/GO composite coatings on the aluminum surface is observed using the SEM in Figure 4. In Figure 4(a), analysis reveals a smooth surface for the 100% pure PI film protective coating. As presented in Figure 4(b)–(e), the coatings with different GO wt% added to the PI films also reveal smooth surfaces without any apparent flaws. The homogeneous and substantial microstructure of the coatings effectively hinders the entrance of corrosive ions. However, a modification homogeneity is noticeable in Figure 4(d) and (e) due to the higher wt% of GO nanoparticles. This leads to non-uniform distribution across the sample surface, resulting in the development of a cotton flocculent structure. By comparing PI and PI/GO composite coatings of Figure 4(a)–(c), the roughness of the PI/GO composites coated samples shown in Figure 4(d) and (e) is evident due to higher GO wt%. Nevertheless, all developed coatings are evenly dispersed across the surface, illustrating that the GO incorporation improves the dispersion of PI within the system. At 50 μm magnification, the surface morphologies of GO/PI composites are far better than the recently reported study [49]. The inclusion of dispersed GO nanoparticles complicates the diffusion pathway for corrosive ions, effectively elongating the course of corrosive ions to reach the aluminum surface. Therefore, the metal substrate attains enhanced protection.

3.4 Crystal structure analysis

XRD examination of PI/GO composites reveals specific diffraction patterns for crystallographic planes (002), (110), and (004), marking the presence of graphite-like structures and the arrangement of graphene layers within the composite. Variations in these planes' diffraction angles or

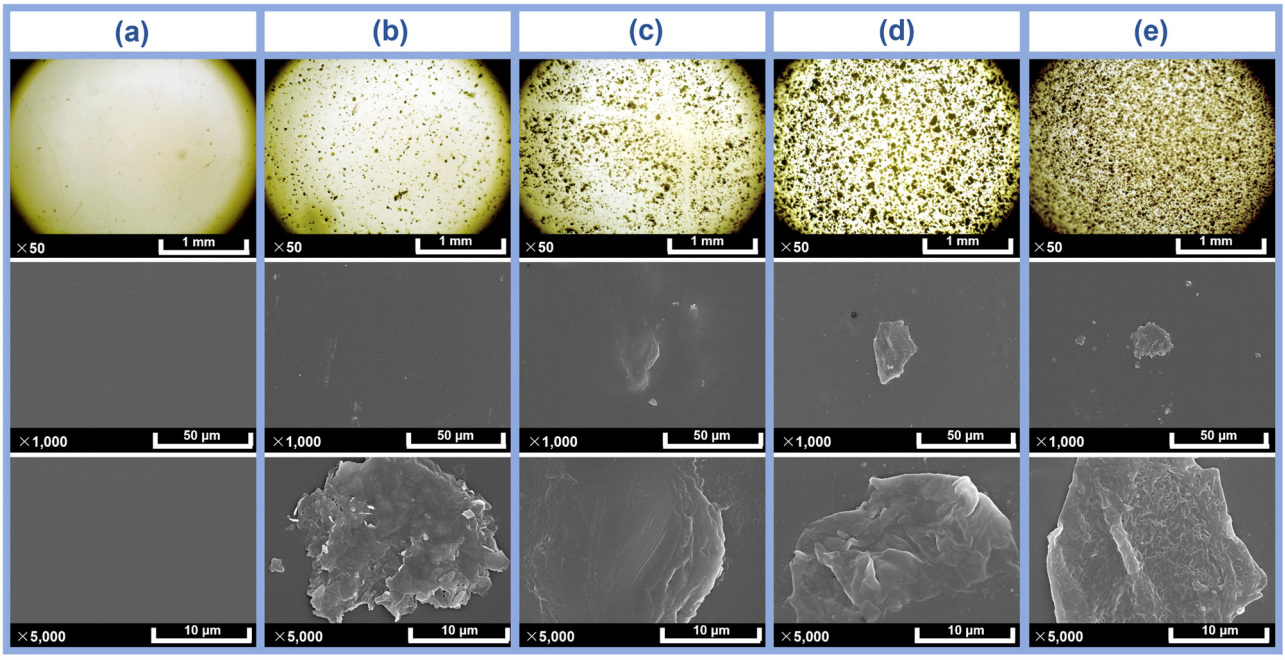

Figure 4: SEM micrographs of PI and PI/GO composites at different resolutions. (a) S_1, (b) S_3, (c) S_4, (d) S_5, (e) S_6.

intensities indicate changes in interlayer spacing and molecular arrangements induced by GO doping. These alterations impact crucial material properties such as conductivity, crystallinity, and mechanical strength.

Figure 5 shows the diffraction patterns of GO/PI composites containing various levels of GO. The occurrence of the diffraction peak near 26 degrees signifies the emergence of (002) planes, while the presence of the (004) peak confirms the establishment of a graphite structure.

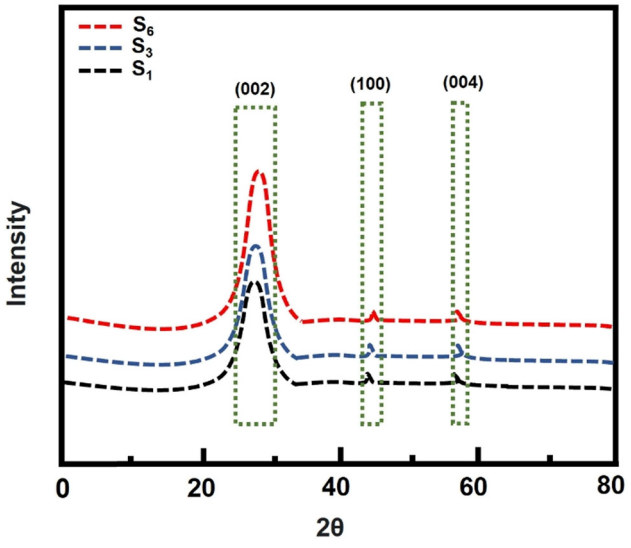

Figure 5: XRD pattern for PI/GO composites.

The (110) plane represents another specific set of crystallographic planes within the lattice structure. In a composite material like PI/GO, these planes could refer to specific orientations or arrangements of atoms or molecular structures. The diffraction peaks related to these planes provide information about their presence and arrangement within the material. As the GO content rises, the angle of diffraction for (002) shifts to a higher degree, signifying a reduction in d_{002}, thus suggesting that GO doping prompts crystallization. It is observed that the GO doping triggers the amplification of graphite crystallite dimensions.

The extensive surface area of GO seems to serve as a crucial catalyst for initiating the crystallization of graphite fibers. As previously discussed, the molecular chains of PI adhered to the graphene sheets and underwent graphitization, transforming into a graphene network during the process. Continuing through graphitization, the layers of graphene sheets expanded, indicating the progressive formation of graphite crystallites. The rise in GO content directly correlated with an escalation in the degree of graphitization, substantiating our initial conjecture.

3.5 EIS analysis of PI/GO composite coatings

Figure 6 illustrates the relationship between the impedance modulus, phase angle, and frequency of composite coating systems. The corrosion resistance of the coating is

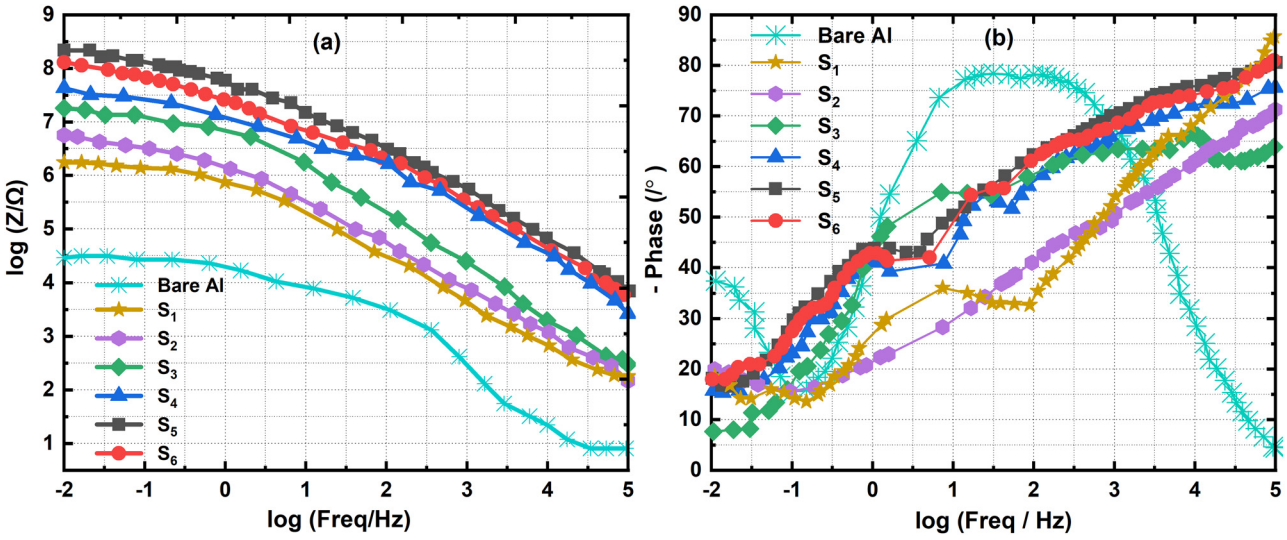

Figure 6: Bode diagrams of bare Al, Pristine PI, and PI/GO composite coatings for anti-corrosion analysis: (a) logarithmic resistivity versus logarithmic frequency curve and (b) phase angle versus logarithmic frequency curve.

significantly influenced by the impedance value in the low-frequency band. The performance of corrosion resistance in the coatings is reflected by the magnitude of its low-frequency impedance modulus, as highlighted in previous research [50]. In Figure 6, it is observed that the impedance of samples coated with various GO wt% exhibit a remarkable surge achieving several orders of magnitude at lower frequencies when compared with the untreated samples. Furthermore, the impedance modulus of the PI/GO composite surpassed three orders of magnitude, reaching a pinnacle of 10^8 cm^2 at a 5 wt% GO. This achievement is significant when considering the contrast with previous findings [51], as it clearly underscores a more than one order enhancement in the low-frequency impedance modulus.

In the midway frequency range of Figure 6, a single high-phase angle peak was observed for bare aluminum, likely arising from the parallel influence of alumina and surface corrosion processes [52]. However, PI/GO coating systems showed a broad phase angle peak in a wide frequency band. It demonstrated that the metal matrix was somewhat shielded from corrosion ions and that the PI/GO coating systems had stronger barriers to corrosive medium. Referring to Figure 6(a), the increase in frequency from −2 to 5 Hz causes a decrease in values of logarithmic resistance for all samples. It can be seen from the curves of Figure 6(a) that the addition of nano-GO wt% in PI matrix improves the logarithmic resistance of samples. The improvement in logarithmic resistance was highest for sample S_5 (5% nano-GO) whereas, the addition of nano-GO in PI films showed much-improved results than bare aluminum. Referring to Figure 6(b), with increasing frequency, i.e., from −2 to 5 Hz the GO is significant in increasing phase angle with increasing GO wt %. The phase angle was recorded highest for sample S_5 (5% nano-GO), whereas S_4 (1% nano-GO) and S_6 (10% nano-GO) showed comparable rise in the phase angles. Moreover, all the samples having nano-GO had more phase angles than bare aluminum showing the impact of nano-GO in PI films.

Figure 7 depicts distinctive capacitive resistance arc configurations for various systems, highlighting their unique equivalent circuits and corrosion resistance mechanisms. Notably, the presence of two capacitive reactance arcs, linked to distinct time constants, reveals significant differences among these systems. Particularly, noteworthy is the substantial superiority of the S_5 coating system capacitive reactance arc compared to the

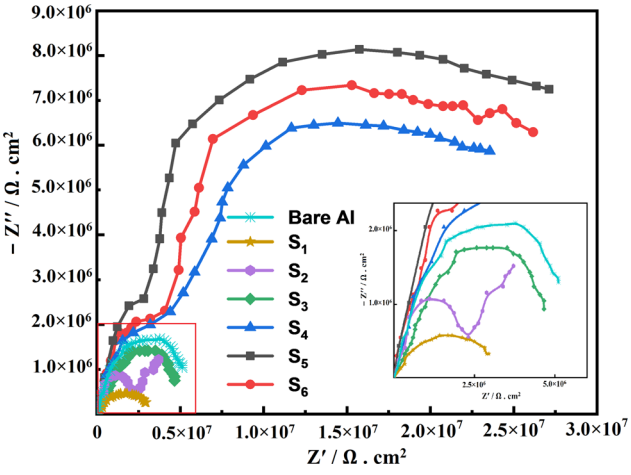

Figure 7: Nyquist plots for bare Al, Pristine PI, and PI/GO composite coatings for anti-corrosion analysis.

others. In the high-frequency range, the coating resistance and capacitance are linked to the capacitive reactance arc, while the lower-frequency range is associated with both charge transfer and solution resistance. A bigger capacitive-reactance arc indicates that the coating is more resistant to corrosion [53].

Enhanced corrosion resistance of the PI/GO composite coatings is indicated by a notable expansion of the capacitive reactance arc. In the context of a 5 wt% GO, as shown in Figure 7, this arc exhibited substantial enlargement compared to other GO concentrations, thus confirming the coating's optimal anti-corrosive efficacy. To investigate deeper into the anti-corrosion mechanism of the PI/GO coating system, the data from experiments were evaluated and an appropriate equal circuit was discerned through the utilization of ZSimDemo software. The fitting parameters for various coating systems are shown in Table 2. In Figure 7, the analogous circuit for PI and PI/GO composites portrays the anticorrosion mechanisms within the coating system.

In this circuit, C_e indicates the capacitance, while R_s specifies the solution resistance, situated among the working electrodes and the electrolytes. The phase element constant (Q) indicates the resistance of the outer layer of the coating along with R_c (the coating resistance) and can be thought of as a particular coating capacitor with poor surface roughness [50]. The charge transfer resistance, or R_{cr}, is an important measure to describe the coating's resistance characteristics. Its value describes the movement of electrons across the surface. According to Figure 8, the R_{cr} of the coatings with various GO contents all exceeds 10^6 and for sample S_5 it was further increased by 10^7 showed strong resistance values, and consequently provided a greater level of protection for the metal matrix. The coating resistance of sample S_5 was far better than the samples prepared in a recent research study [54]. The resistance of the inner layer of the coating is represented by the double-layer capacitance (C_{dl}) and resistance (R_{dl}) [55–57].

In Table 2, with the increase in nano-GO in PI films the value of series resistance R_s increases. The maximum value

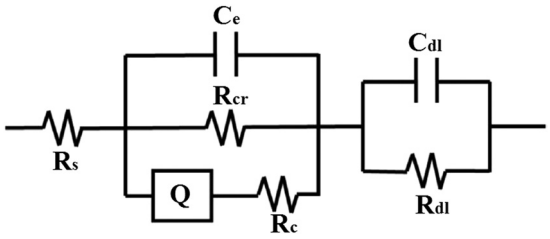

Figure 8: Equivalent circuit illustration for Pristine PI, and PI/GO composites with varying GO wt% coatings.

of 512.5 Ω cm^2 was recorded for sample S_5 followed by 231.9 and 198.3 Ω cm^2 for samples S_6 and S_4, respectively. Moreover, the other resistances R_{cr}, R_c, and R_{dl} followed the same trend. The increase in values of resistance is attributed to the increased anti-corrosion ability of PI/GO composites having varied nano-GO compositions. Moreover, the decrease in values of C_e was recorded for each composite having nano-GO. The lowest value of 4.6×10^{-10} F cm^{-2} was recorded for sample S_5 which showed the highest anti-corrosion ability of this sample. The capacitance of other samples S_6 and S_4 had 8.5×10^{-10} and 9.5×10^{-10} F cm^{-2}, respectively. This result elucidates that the impact of nano-GO in PI films can enhance the anti-corrosion abilities up to a certain concentration (5% nano-GO), further increase in nano-GO in the PI film reduces the anti-corrosion ability of these composites.

3.6 Tafel analysis of PI/GO composite coatings

The Tafel curve of PI and PI/GO composites is illustrated in Figure 9 and the corrosion parameters are listed in Table 3. The current density (I_{cor}) illustrates the immediate rate of corrosion reaction from the kinetics prospect and corrosion potential (E_{cor}) signifies the corrosion tendency of materials from the thermodynamics prospect [54]. To vividly illustrate the protective impact of different systems of coating on an

Table 2: Equivalent circuit parameters for pristine PI, and PI/GO composites with varying GO wt% coatings

Sample	C_e (F cm^{-2})	R_s (Ω cm^2)	R_{cr} (Ω cm^2)	Q Y_o (Ω^{-1} sn cm^{-2})	n	R_c (Ω cm^2)	R_{dl} (Ω cm^2)	C_{dl} (Ω cm^2)
S_1	3.5×10^{-9}	92.5	2.2×10^6	3.4×10^{-7}	0.7	1.6×10^4	2.1×10^3	2.5×10^{-9}
S_2	2.8×10^{-9}	104.2	5.8×10^6	2.1×10^{-7}	0.8	4.1×10^3	3.5×10^2	1.2×10^{-8}
S_3	1.5×10^{-9}	145.8	8.9×10^6	1.1×10^{-7}	0.6	9.5×10^3	4.6×10^3	3.5×10^{-9}
S_4	9.5×10^{-10}	198.3	1.6×10^7	7.4×10^{-8}	0.5	4.5×10^3	8.2×10^4	2.9×10^{-8}
S_5	4.6×10^{-10}	512.5	6.1×10^7	2.2×10^{-8}	0.4	1.1×10^2	9.6×10^5	2.2×10^{-8}
S_6	8.5×10^{-10}	231.9	3.2×10^6	4.4×10^{-8}	0.5	3.5×10^3	4.1×10^6	3.5×10^{-7}

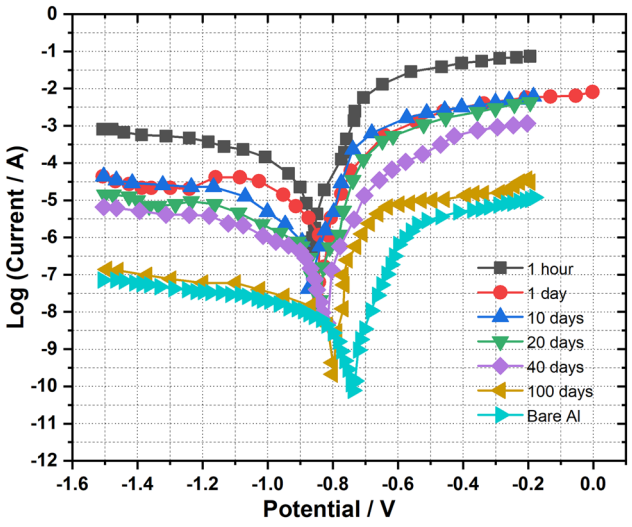

Figure 9: Investigating current density (I_{cor}) and corrosion potential (E_{cor}) by Tafel curve of bare Al, pristine PI, and PI/GO composite coatings.

aluminum alloy substrate, the protection efficiency (η) of the coatings was estimated by utilizing the following equation:

$$\eta = \frac{I_{cor1} - I_{cor2}}{I_{cor1}}, \quad (1)$$

where I_{cor1} and I_{cor2} represent I_{cor} of bare aluminum and PI/GO composite coatings, respectively.

Figure 9 signifies that the E_{cor} of S_5 coating system was 0.78 V which is 80 mV higher in the positive direction than the E_{cor} of bare aluminum, i.e., 0.86 V. Also, the I_{cor} of the S_5 surface coating system is more than 2 orders of magnitude lower than that of pure aluminum. This confirmed that the rate of corrosion is relatively low and could effectively protect the matrix. The values of I_{cor} for all samples prepared in this work are much higher than the samples used in the recent study [58,59]. The strongest protective effect on the aluminum matrix is attained when the 5 wt% GO is incorporated in the PI matrix, as shown in Figure 9 and the I_{cor} reached 4.8×10^{-9} A cm^{-2}. Table 3 depicts the calculation

Table 3: Polarization parameters of bare Al, pristine PI, and PI/GO composite coatings

Sample	I_{cor} (A cm^{-2})	E_{cor} (V)	R_p (Ω cm^2)	η (%)
Bare Al	8.5×10^{-6}	−0.86	2.0×10^{3}	
S_1	1.1×10^{-7}	−0.85	8.9×10^{4}	98.5954
S_2	2.8×10^{-7}	−0.84	9.8×10^{4}	99.9545
S_3	5.4×10^{-8}	−0.82	4.6×10^{5}	99.9885
S_4	8.8×10^{-9}	−0.80	2.8×10^{6}	99.9902
S_5	4.8×10^{-9}	−0.78	6.1×10^{6}	99.9998
S_6	7.4×10^{-9}	−0.79	4.2×10^{6}	99.9991

of experimental findings of bare aluminum, pristine PI, and PI/GO composite coating systems. It was found that each coating on the aluminum substrate had a protective efficiency of over 99%. When the GO concentration was 5 wt%, the best protection efficiency was 99.9998%. Moreover, the resistance R_p was increased with the increase of nano-GO content in PI films. The highest resistance of 6.1×10^6 Ω cm^2 was recorded for sample S_5 which was again attributed to its optimum inclusion of 5% nano-GO into PI films. The other samples having nano-GO showed better anti-corrosion resistance compared with bare aluminum and pristine PI film.

3.7 EIS analysis of PI/GO composite coatings after NaCl immersion test

The NaCl immersion test was performed on S_3 and S_5 samples to observe the long-term reliability of developed coatings. Figure 10 demonstrates the electrochemical analysis of the S_3 and S_5 coatings after immersion in a 3.5 wt% NaCl solution. Compared to the impedance of the S_3 coating after 1 h of immersion, the coating's impedance reduced to 10^7 cm² after one day of immersion. Following 10 days of immersion, changes in the impedance frequency curve shape were observed, and the impedance modulus of the surface coating was reduced to slightly above 10^5 cm² (Figure 10(a)). The curve of frequency related to phase angle has undergone alterations, revealing two discernible peaks upon a thorough examination of Figure 10(b). The observations indicate that corrosion ions infiltrated the coating's surface, causing erosion, while corrosion products accumulated, leading to a modification in the protection process of the surface coating on the metal alloy substrate. Also, following 100 days of immersion, the coating's impedance module at low frequencies almost approached the level seen in bare aluminum. The phase angle frequency curve has undergone further changes in comparison to the 20-day immersion, as depicted in Figure 10(b). Especially, a broader peak emerged within the medium frequency range, replacing the previous two peaks. This observation suggests the potential infiltration of corrosion ions in the inner system of the protective coating, their traversal within the coating, and eventual interaction with the metal alloy substrate, leading to metal corrosion while concurrently accumulating more corrosive by-products on the outer surface of the coating. On the other hand, in Figure 10(c), the S_5 coating, which demonstrated superior performance, exhibited an impedance of 10^8 after just 1 h of immersion. Impressively, this coating's efficacy endured

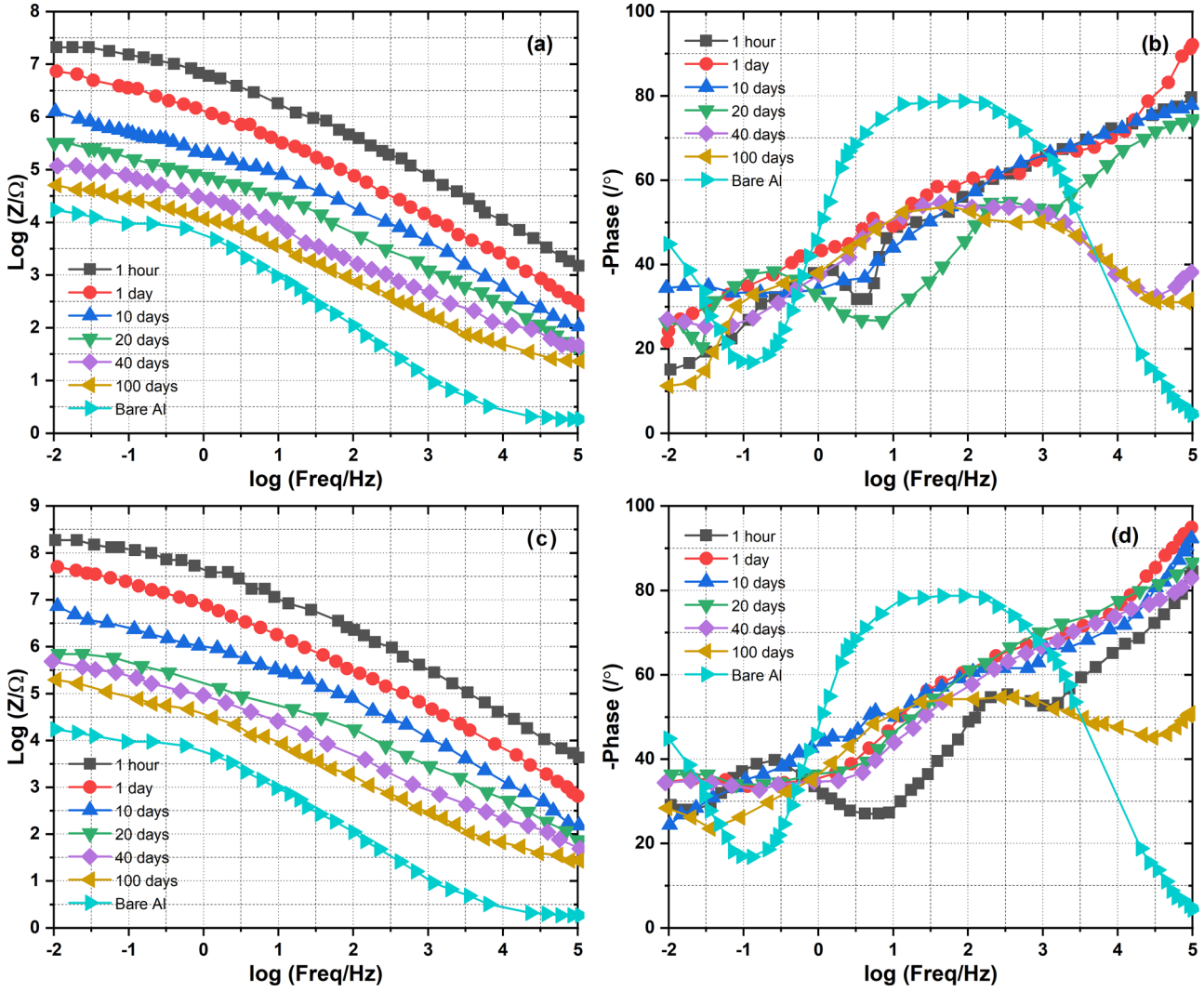

Figure 10: Bode diagram of coatings after immersion in NaCl solution in comparison with bare aluminum: (a) logarithmic curve of resistivity versus frequency of S_3, (b) difference in phase angle versus frequency range of S_3, (c) logarithmic curve of resistivity versus frequency of S_5, and (d) difference in phase angle versus frequency range of S_3.

even after 100 h of exposure to the NaCl solution, with its impedance value nearly tenfold higher than that of bare aluminum. This substantial improvement highlights the favorable performance of the nano-GO composition. Thus, it can be asserted that the current level of protection this coating offers for the metal substrate surpasses that of previously employed coatings [24].

4 Conclusions

Successfully manufactured, the PI/GO composite coatings serve as an effective shield against corrosion for aluminum alloy substrates. The infusion of GO within the PI matrix leads to increased contact angles and a roughened surface, advancing hydrophobicity and resistance against corrosion. This incorporation ensures a uniform, compact surface that firmly adheres to the metal substrate. With an optimal GO concentration of 5 wt%, the low-frequency impedance modulus experiences an exponential three-order increase, reaching an impressive 10^8 cm^2 in comparison to bare aluminum. Demonstrated by the polarization curve, the corrosion current (I_{cor}) witnesses a remarkable reduction of nearly three orders of magnitude, registering at 4.8×10^{-9} A cm^{-2}. Immersion tests in a 3.5 wt% NaCl solution exhibit the extraordinary durability of the composite coating, showcasing its ability to withstand corrosion for up to 100 days. This strategic integration of GO within the PI matrix strengthens the aluminum alloy substrate, significantly improving its properties and extending its

lifespan in moist environments. Prospects for GO/PI composite coatings in the future include improved durability, low production costs, and customized formulations for a range of applications. The potential for revolutionizing corrosion protection across industries lies in the integration of smart coatings with sensing capabilities for real-time corrosion monitoring. These coatings have exceptional hydrophobicity, electrical conductivity, and corrosion resistance, making them suitable for applications in industrial machinery, oil and gas equipment, automobile parts, marine vessels, aerospace structures, and infrastructure. By providing protection from moisture, salt, chemicals, and contaminants, these coatings increase asset longevity, lower maintenance costs, and guarantee operational dependability.

Acknowledgments: The authors acknowledge the support of the Department of Education of Guangxi Autonomous Region under grant number 2023KY0826. This work was funded by the Researchers Supporting Project Number (RSP2024R267), King Saud University, Riyadh, Saudi Arabia.

Funding information: This work was supported by the Department of Education of Guangxi Autonomous Region under grant number 2023KY0826. This work was funded by the Researchers Supporting Project Number (RSP2024R267), King Saud University, Riyadh, Saudi Arabia.

Author contributions: All authors have accepted responsibility for the entire content of this manuscript and approved its submission.

Conflict of interest: The authors state no conflict of interest.

Data availability statement: The datasets generated and/or analysed during the current study are available from the corresponding author on reasonable request.

References

[1] Li YT, Chen XM, Zeng XK, Liu M, Jiang X, Leng YX. Hard yet tough and self-lubricating (CuNiTiNbCr) Cx high-entropy nanocomposite films: Effects of carbon content on structure and properties. J Mater Sci Technol. 2024 Feb;173:20–30.

[2] Zhao X, Fan B, Qiao N, Soomro RA, Zhang R, Xu B. Stabilized Ti3C2Tx-doped 3D vesicle polypyrrole coating for efficient protection toward copper in artificial seawater. Appl Surf Sci. 2024 Jan;642:158639.

[3] Kuang W, Wang H, Li X, Zhang J, Zhou Q, Zhao Y. Application of the thermodynamic extremal principle to diffusion-controlled phase transformations in Fe-CX alloys: Modeling and applications. Acta Mater. 2018 Oct;159:16–30.

[4] Meng B, Wang J, Chen M, Zhu S, Wang F. Study on the oxidation behavior of a novel thermal barrier coating system using the nanocrystalline coating as bonding coating on the single-crystal superalloy. Corros Sci. 2023 Dec;225:111591.

[5] Xie J, Chen Y, Yin L, Zhang T, Wang S, Wang L. Microstructure and mechanical properties of ultrasonic spot welding TiNi/Ti6Al4V dissimilar materials using pure Al coating. J Manuf Process. 2021 Apr;64:473–80.

[6] Yin S, Du Y, Liang X, Xie Y, Xie D, Mei Y. Surface coating of biomass-modified black phosphorus enhances flame retardancy of rigid polyurethane foam and its synergistic mechanism. Appl Surf Sci. 2023 Nov;637:157961.

[7] Refait P, Jeannin M, Sabot R, Antony H, Pineau S. Corrosion and cathodic protection of carbon steel in the tidal zone: Products, mechanisms and kinetics. Corros Sci. 2015 Jan 1;90:375–82.

[8] Ituen E, James A, Akaranta O, Sun S. Eco-friendly corrosion inhibitor from Pennisetum purpureum biomass and synergistic intensifiers for mild steel. Chin J Chem Eng. 2016 Oct;24(10):1442–7.

[9] Abd El Wanees S, Radwan AB, Alsharif MA, Abd El Haleem SM. Initiation and inhibition of pitting corrosion on reinforcing steel under natural corrosion conditions. Mater Chem Phys. 2017 Apr;190:79–95.

[10] Papanicolaou GC, Kontaxis LC, Portan DV, Petropoulos GN, Valeriou E, Alexandropoulos D. Mechanical performance enhancement of aluminum Single-Lap adhesive joints due to organized alumina nanotubes layer formation on the aluminum adherends. Appl Nano. 2021 Aug;2(3):206–21.

[11] Yin S, Ren X, Zheng R, Li Y, Zhao J, Xie D, et al. Improving fire safety and mechanical properties of waterborne polyurethane by montmorillonite-passivated black phosphorus. Chem Eng J. 2023 May;464:142683.

[12] Li YT, Jiang X, Wang XT, Leng YX. Integration of hardness and toughness in (CuNiTiNbCr) Nx high entropy films through nitrogen-induced nanocomposite structure. Scr Mater. 2024 Jan;238:115763.

[13] Pourhashem S, Saba F, Duan J, Rashidi A, Guan F, Nezhad EG, et al. Polymer/Inorganic nanocomposite coatings with superior corrosion protection performance: A review. J Ind Eng Chem. 2020 Aug;88:29–57.

[14] Bakshi MI, Ahmad S. In-situ synthesis of synergistically active ceria doped polypyrrole oleo-polyesteramide hybrid nanocomposite coatings: Corrosion protection and flame retardancy behaviour. Prog Org Coat. 2020 Oct;147:105778.

[15] Jeong N, Jwa E, Kim C, Choi JY, Nam JY, Hwang KS, et al. One-pot large-area synthesis of graphitic filamentous nanocarbon-aligned carbon thin layer/carbon nanotube forest hybrid thin films and their corrosion behaviors in simulated seawater condition. Chem Eng J. 2017 Apr;314:69–79.

[16] Zhu S, Zhu J, Ye S, Yang K, Li M, Wang H, et al. High-entropy rare earth titanates with low thermal conductivity designed by lattice distortion. J Am Ceram Soc. 2023 Oct;106(10):6279–91.

[17] Wang K, Zhu J, Wang H, Yang K, Zhu Y, Qing Y, et al. Air plasma-sprayed high-entropy (Y0. 2Yb0. 2Lu0. 2Eu0. 2Er0. 2) 3Al5O12 coating with high thermal protection performance. J Adv Ceram. 2022 Oct;11(10):1571–82.

[18] Krebs FC. Fabrication and processing of polymer solar cells: A review of printing and coating techniques. Sol Energy Mater Sol Cell. 2009 Apr;93(4):394–412.

[19] He H, Shi J, Yu S, Yang J, Xu K, He C, et al. Exploring green and efficient zero-dimensional carbon-based inhibitors for carbon steel:

From performance to mechanism. Constr Build Mater. 2024 Jan;411:134334.
[20] Li X, Liu Y, Leng J. Large-scale fabrication of superhydrophobic shape memory composite films for efficient anti-icing and de-icing. Sustain Mater Technol. 2023 Sep;37:e00692.
[21] Ramezanzadeh B, Ahmadi A, Mahdavian MJ. Enhancement of the corrosion protection performance and cathodic delamination resistance of epoxy coating through treatment of steel substrate by a novel nanometric sol-gel based silane composite film filled with functionalized graphene oxide nanosheets. Corros Sci. 2016 Aug;109:182–205.
[22] Parhizkar N, Shahrabi T, Ramezanzadeh B. A new approach for enhancement of the corrosion protection properties and interfacial adhesion bonds between the epoxy coating and steel substrate through surface treatment by covalently modified amino functionalized graphene oxide film. Corros Sci. 2017 Jul;123:55–75.
[23] Langroudi AE, Yousefi AA, Kabiri K. Effect of Silane Coupling Agent on Interfacial Adhesion of Copper/Glass Fabric/Epoxy Com-posites. Iran Polym J. 2003;12(3):201–10.
[24] Ghany NA, Elsherif SA, Handal HT. Revolution of Graphene for different applications: State-of-the-art. Surf Interfaces. 2017 Dec;9:93–106.
[25] Esfahani SL, Rouhani S, Ranjbar Z. Optimization the electrophoretic deposition fabrication of graphene-based electrode to consider electro-optical applications. Surf Interfaces. 2017 Dec;9:218–27.
[26] Choi HJ, Jung SM, Seo JM, Chang DW, Dai L, Baek JB. Graphene for energy conversion and storage in fuel cells and supercapacitors. Nano Energy. 2012 Jul;1(4):534–51.
[27] Kuhn L, Gorji NE. Review on the graphene/nanotube application in thin film solar cells. Mater Lett. 2016 May;171:323–6.
[28] Gupta VK, Yola ML, Atar N, Ustundağ Z, Solak AO. A novel sensitive Cu (II) and Cd (II) nanosensor platform: graphene oxide terminated p-aminophenyl modified glassy carbon surface. Electrochim Acta. 2013 Dec;112:541–8.
[29] Yola ML, Atar N, Üstündağ Z, Solak AO. A novel voltammetric sensor based on p-aminothiophenol functionalized graphene oxide/gold nanoparticles for determining quercetin in the presence of ascorbic acid. J Electroanal Chem. 2013 Jun;698:9–16.
[30] Yola ML, Gupta VK, Eren T, Şen AE, Atar N. A novel electro analytical nanosensor based on graphene oxide/silver nanoparticles for simultaneous determination of quercetin and morin. Electrochim Acta. 2014 Feb;120:204–11.
[31] Zhou P, Li W, Zhu X, Li Y, Jin X, Chen J. Graphene containing composite coatings as a protective coatings against hydrogen embrittlement in quenching & partitioning high strength steel. J Electrochem Soc. 2016 Jan;163(5):D160.
[32] Yoo BM, Shin HJ, Yoon HW, Park HB. Graphene and graphene oxide and their uses in barrier polymers. J Appl Polym Sci. 2014 Jan;131(1).
[33] Ramezanzadeh B, Ghasemi E, Mahdavian M, Changizi E, Moghadam MM. Covalently-grafted graphene oxide nanosheets to improve barrier and corrosion protection properties of polyurethane coatings. Carbon. 2015 Nov;93:555–73.
[34] Lee W, Lee JU, Jung BM, Byun JH, Yi JW, Lee SB, et al. Simultaneous enhancement of mechanical, electrical and thermal properties of graphene oxide paper by embedding dopamine. Carbon. 2013 Dec;65:296–304.
[35] Yousefi N, Lin X, Zheng Q, Shen X, Pothnis JR, Jia J, et al. Simultaneous in situ reduction, self-alignment and covalent bonding in graphene oxide/epoxy composites. Carbon. 2013 Aug;59:406–17.
[36] Zhu X, Yan Q, Cheng L, Wu H, Zhao H, Wang L. Self-alignment of cationic graphene oxide nanosheets for anticorrosive reinforcement of epoxy coatings. Chem Eng J. 2020 Jun;389:124435.
[37] Cui G, Bi Z, Zhang R, Liu J, Yu X, Li Z. A comprehensive review on graphene-based anti-corrosive coatings. Chem Eng J. 2019 Oct;373:104–21.
[38] Korshak VV, Khomutov VA, Doroshenko YY. A study of thermal stability in a number of aromatic and nitrogen containing polycyclic compounds. Polym Sci USSR. 1976 Jan;18(3):597–603.
[39] Liu Y, Huang J, Tan J, Zeng Y, Liu J, Zhang H, et al. Intrinsic high-barrier polyimide with low free volume derived from a novel diamine monomer containing rigid planar moiety. Polymer. 2017 Apr;114:289–97.
[40] Lei X, Chen Y, Qiao M, Tian L, Zhang Q. Hyperbranched polysiloxane (HBPSi)-based polyimide films with ultralow dielectric permittivity, desirable mechanical and thermal properties. J Mater Chem C. 2016;4(11):2134–46.
[41] Tsai MH, Huang SL, Chiang PC, Chen CJ. Morphology, dynamic mechanical properties, and gas separation of crosslinking silica-containing polyimide nanocomposite thin film. J Appl Polym Sci. 2007 Dec;106(5):3185–92.
[42] Huang TC, Yeh LC, Lai GH, Huang BS, Yang TI, Hsu SC, et al. Advanced superhydrophobic electroactive fluorinated polyimide and its application in anticorrosion coating. Int J Green Energy. 2017 Jan;14(2):113–20.
[43] Dorigato A, Pegoretti A. Development and thermo-mechanical behavior of nanocomposite epoxy adhesives. Polym Adv Technol. 2012 Mar;23(3):660–8.
[44] Gul S, Kausar A, Mehmood M, Muhammad B, Jabeen S. Progress on epoxy/polyamide and inorganic nanofiller-based hybrids: introduction, application, and future potential. Polym Technol Eng. 2016 Nov;55(17):1842–62.
[45] Tang S, Lei B, Feng Z, Guo H, Zhang P, Meng G. Progress in the Graphene Oxide-Based Composite Coatings for Anticorrosion of Metal Materials. Coatings. 2023 Jun;13(6):1120.
[46] Ahmed M, Zhong L, Li F, Xu N, Gao J. Improving the DC dielectric properties of XLPE with appropriate content of dicumyl peroxide for HVDC cables insulation. Materials. 2022 Aug;15(17):5857.
[47] Yuan Z, Bin J, Wang M, Huang J, Peng C, Xing S, et al. Preparation of a polydimethylsiloxane (PDMS)/CaCO3 based superhydrophobic coating. Surf Coat Technol. 2014 Sep;254:97–103.
[48] Zhang J, Zhang Z, Jiao Y, Yang H, Li Y, Zhang J, et al. The graphene/lanthanum oxide nanocomposites as electrode materials of supercapacitors. J Power Sources. 2019 Apr;419:99–105.
[49] Ali MR, Chowdhury MA, Shahin M, Rahman MM, Ali MO, Gafur MA. Multi-physical and anti-corrosion properties of graphene-reinforced epoxy nanocomposite coatings for industrial applications. Arab J Chem. 2024 Jan;17(1):105424.
[50] Li L, He J, Lei J, Xu W, Jing X, Ou X, et al. A sol–bath–gel approach to prepare hybrid coating for corrosion protection of aluminum alloy. Surf Coat Technol. 2015 Oct;279:72–8.
[51] Zhu G, Cui X, Zhang Y, Chen S, Dong M, Liu H, et al. Poly (vinyl butyral)/graphene oxide/poly (methylhydrosiloxane) nanocomposite coating for improved aluminum alloy anticorrosion. Polymer. 2019 May;172:415–22.
[52] Cui X, Zhu G, Pan Y, Shao Q, Dong M, Zhang Y, et al. Polydimethylsiloxane-titania nanocomposite coating: Fabrication and corrosion resistance. Polymer. 2018 Feb;138:203–10.

[53] Liu S, Gu L, Zhao H, Chen J, Yu H. Corrosion resistance of graphene-reinforced waterborne epoxy coatings. J Mater Sci & Technol. 2016 May;32(5):425–31.
[54] Keramatinia M, Ramezanzadeh B, Mahdavian M. N-doped-GO@ Zn nano-layers filled epoxy composite with superior mechanical and anti-corrosion properties. Colloids Surf A: Physicochem Eng Asp. 2024 Jan;681:132743.
[55] Li J, Ge S, Wang J, Du H, Song K, Fei Z, et al. Water-based rust converter and its polymer composites for surface anticorrosion. Colloids Surf A: Physicochem Eng Asp. 2018 Jan;537:334–42.
[56] Chaudhry AU, Mansoor B, Mungole T, Ayoub G, Field DP. Corrosion mechanism in PVD deposited nano-scale titanium nitride thin film with intercalated titanium for protecting the surface of silicon. Electrochim Acta. 2018 Feb;264:69–82.
[57] Torrico RF, Harb SV, Trentin A, Uvida MC, Pulcinelli SH, Santilli CV, et al. Structure and properties of epoxy-siloxane-silica nanocomposite coatings for corrosion protection. J Colloid Interface Sci. 2018 Mar;513:617–28.
[58] Cao Y, Zheng D, Li X, Lin J, Wang C, Dong S, et al. Enhanced corrosion resistance of superhydrophobic layered double hydroxide films with long-term stability on Al substrate. ACS Appl Mater Interfaces. 2018 Apr;10(17):15150–62.
[59] Pandey U, Kumar A, Sharma C. Comprehensive anti-corrosion study of electrodeposited graphene oxide-alumina composite with nickel matrix in NaCl solution. Diam Relat Mater. 2024 Jan;141:110653.